Baek *et al. Appl Adhes Sci (2017) 5:4*
DOI 10.1186/s40563-017-0082-z

Applied Adhesion Science

RESEARCH Open Access

Evaluation of energy dissipation involving adhesion hysteresis in spherical contact between a glass lens and a PDMS block

Dooyoung Baek[1*], Pasomphone Hemthavy[2], Shigeki Saito[2] and Kunio Takahashi[2]

*Correspondence:
baek.d.aa@m.titech.ac.jp;
baek.s.dy@gmail.com
[1] Department of International Development Engineering, Tokyo Institute of Technology, 2-12-1 O-okayama, Meguro-ku, Tokyo 152-8552, Japan
Full list of author information is available at the end of the article

Abstract

Adhesion hysteresis was investigated with the energy dissipation in the contact experiments between a spherical glass lens and a polydimethylsiloxane (PDMS) block. The experiments were conducted under step-by-step loading–unloading for the spontaneous energy dissipation. The force, contact radius, and displacement were measured simultaneously and the elasticity of the PDMS was confirmed. The work of adhesion was estimated in the loading process of the strain energy release rate. The total energy dissipation has been observed to be linearly proportional to the contact radius in the unloading process. The approximately constant gradient of the energy dissipation for each unloading process has been found. The result would provide how the dissipation is induced during the unloading as some interfacial phenomena. The fact has been discussed with some interfacial phenomena, e.g., the adsorbates on the surface, for the mechanism of adhesion hysteresis.

Keywords: Adhesion by physical adsorption, Adhesion hysteresis, Energy dissipation

Background

Adhesion phenomena in contact problems using elastomers and soft materials play a significant role in design of devices, e.g., microfabricated adhesives [1–3] and wall-climbing robots [4, 5]. Theory of adhesive elastic contact [6–8] considering both of the elastic deformation and adhesion phenomenon in contact interface between elastic bodies is helpful for its applications. Since the adhesive elastic contact theory assumes the total energy equilibrium, contact process in the theory (i.e., consists of loading–unloading or advancing-receding contact) is reversible except for its mechanical hysteresis [9]. However, it has been reported that adhesion hysteresis exists in some contact experiments [10–21]. This adhesion hysteresis shows a completely different force curve (force–displacement or force-contact area) between loading–unloading or advancing-receding in actual contact process. Adhesion hysteresis means that the actual contact process is not in equilibrium as assumed in the theory and also means that the total energy in the contact system is dissipated during the process. Therefore, investigating the energy dissipation is significant for understanding the mechanism and complementing the conventional theory.

The energy dissipation in the adhesive contact is mainly investigated and discussed using the strain energy release rate G (i.e., the energy required to separate unit contact area J/m^2) [9–18]. Maugis and Barquins [10] first introduced a concept of linear elastic fracture mechanics into the Johnson–Kendall–Roberts (JKR) contact [6]. They experimentally showed that G has a dependency on the crack speed [10], which is the so-called empirical relationship [11–14]. However, the relationship does not represent how the total energy dissipation changes during the contact process, and the mechanism of adhesion hysteresis is still on discussion assuming capillary condensation or adsorbed layer, etc. [17–19, 22–25]. In this paper, a polydimethylsiloxane (PDMS) block is used as the elastic materials, the contact processes between the PDMS and a glass lens have been investigated to evaluate the energy dissipation. Especially, the change in the energy dissipation during the processes is discussed using the elastic contact theory, assuming non-equilibrium.

Methods

Contact mechanics for evaluating energy dissipation

Figure 1 shows a schematic illustration of the spherical contact model describing contact between the spherical rigid tip and the elastic body considering the equivalent stiffness in the measurement system, e.g., a cantilever-like structure, a strain gauge force sensor, and etc. in an actual measurement system. Total energy U_{total} of the contact model is given by Takahashi et al. [7], who described the contact mechanics considering the equivalent stiffness based on the JKR theory [6]. The model assumes small deformation, linear elasticity, elastic half-space, and frictionless surfaces. Moreover, in this study the external work given by the movement of the gross displacement Z is transferred instantaneously and fully to the contact system. Hence, the total energy U_{total} is spontaneously dissipated toward an equilibrium at a fixed Z. The dissipated energy $\Delta U_{\text{dissipation}}$ (i.e., same as a negative increment of total energy $-\Delta U_{\text{total}}$ in the contact system) at a fixed Z is expressed as

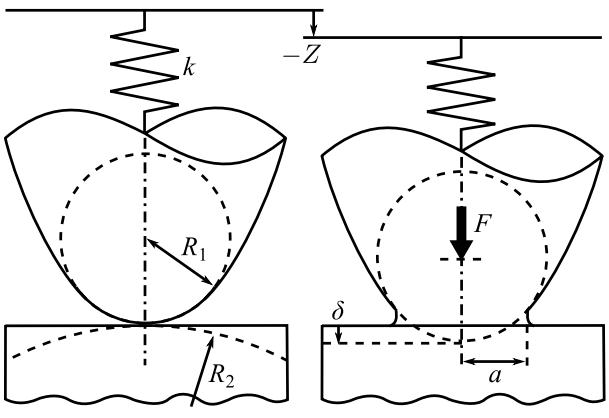

Fig. 1 Schematic illustration of the spherical contact model, where Z is the gross displacement controlled by the experimental apparatus, k is the equivalent stiffness of the measurement system, R_1 is the radius of curvature of the spherical rigid tip, R_2 is the radius of curvature of the elastic body surface, F is the applied force between the spherical rigid tip and the elastic body, δ is the penetration depth of the spherical rigid tip into the elastic body, and a is the radius of the contact area

$$\Delta U_{\text{dissipation}} = -\Delta U_{\text{total}} = -(\Delta U_{\text{elastic}} + \Delta U_{\text{interface}} + \Delta U_{\text{stiffness}}), \tag{1}$$

where $\Delta U_{\text{elastic}}$ is an increment of the elastic energy stored in the elastic body due to its deformation, $\Delta U_{\text{interface}}$ is an increment of the interface energy stored in the contact area by the work of adhesion, $\Delta U_{\text{stiffness}}$ is an increment of the stiffness energy stored in the spring corresponding to the equivalent stiffness k of the measurement system [7]. In the spherical contact, the stress distribution in the contact area can be described by the linear combination using Hertz's and Boussinesq's stress distribution although the process is not in equilibrium [26, 27]. The specific derivation is given by Muller et al. [26] in the section of the JKR model interpretation. The relationship between the force F, the penetration depth δ, and the contact radius a [26, 27] is given as

$$F = 2E^* a\left(\delta - \frac{a^2}{3R}\right), \tag{2}$$

where $E^* = E/(1-\nu^2)$ is the elastic modulus of the elastic body (ν is the Poisson's ratio), and R is an effective radius of curvature:

$$\frac{1}{R} = \frac{1}{R_1} + \frac{1}{R_2}, \tag{3}$$

where R_1 and R_2 are the radii of curvature of the spherical rigid tip and the elastic body as shown in Fig. 1. The radius of curvature of the elastic body R_2 is infinite when the surface of the elastic body is flat, i.e., $R = R_1$. The force F is also applied to the spring k, which can be expressed by Hooke's law as

$$F = k(-Z - \delta). \tag{4}$$

Therefore, the relationship between the force F, the gross displacement Z, and the contact radius a is obtained from substituting Eq. (4) into Eq. (2):

$$F = \frac{2kE^* a}{2E^* a + k}\left(-Z - \frac{a^2}{3R}\right). \tag{5}$$

Although the adhesion hysteresis is observed in the measurements (F, Z, a), the measurements must satisfy Eq. (5) if a material behaves as an elastic material in the contact experiments. Therefore, Eq. (5) can be used to confirm the elasticity of the material when k, R are given and F, Z, a are measured in the experiments.

The strain energy release rate G_Z at a fixed Z is defined and calculated:

$$\begin{aligned} G_Z &= \left[\frac{\partial U_{\text{elastic}}}{\partial(\pi a^2)} + \frac{\partial U_{\text{stiffness}}}{\partial(\pi a^2)}\right]_Z \\ &= \frac{(4E^* a^3/3R - F)^2}{6\pi R(4E^* a^3/3R)}, \end{aligned} \tag{6}$$

where U_{elastic} and $U_{\text{stiffness}}$ are the components of $U_{\text{total}} = U_{\text{elastic}} + U_{\text{stiffness}} + U_{\text{interface}}$ given by Takahashi et al. [7]:

$$U_{\text{elastic}} = \frac{4E^* a^5}{45R^2} + \frac{F^2}{4E^* a}, \tag{7}$$

$$U_{\text{stiffness}} = \frac{F^2}{2k}, \tag{8}$$

$$U_{\text{interface}} = -\pi a^2 \Delta\gamma. \tag{9}$$

$U_{\text{interface}}$ is the interface energy stored in the contact area, which is contributed by the thermodynamic reversible work of adhesion $\Delta\gamma$ during an entire contact process. The work of adhesion is a material constant of interface defined by Dupré [28]: $\Delta\gamma = \gamma_1 + \gamma_2 - \gamma_{12}$, where γ_1, γ_2 are the surface free energy, γ_{12} is the interface free energy per unit area (J/m^2). The strain energy release rate G_Z is also expressed using Eqs. (1), (6) and (9) as

$$\begin{aligned} G_Z &= \left[-\frac{\partial U_{\text{dissipation}}}{\partial(\pi a^2)} - \frac{\partial U_{\text{interface}}}{\partial(\pi a^2)} \right]_Z \\ &= -\frac{\partial U_{\text{dissipation}}}{2\pi a \partial a} + \Delta\gamma, \end{aligned} \tag{10}$$

which shows that G_Z consists of a dissipative term (variable; $-\partial U_{\text{dissipation}} / 2\pi a \partial a$) and the reversible term (constant; $\Delta\gamma$). It also shows that the energy dissipation is contributed by $G_Z - \Delta\gamma$ (the reversible term is excluded from the required energy to change unit contact area) and the equilibrium of total energy is given as $G_Z = \Delta\gamma$ at the dissipative term to be zero. From Eq. (10), therefore, the total energy dissipation can be evaluated numerically by using the rectangular rule as

$$U_{\text{dissipation}} = \sum \left[-(G_Z(a_{i+1}) - \Delta\gamma)\left(\pi a_{i+1}^2 - \pi a_i^2\right) \right], \tag{11}$$

where a_i is the instantaneous contact radius measured during the time-series measurements, $G_Z(a)$ is a function of a obtained from substituting Eq. (5) into Eq. (6), and the summation is performed over the range of the time-series measurement in the contact experiment.

Spherical contact measurement system

The measurement system was constructed as shown in Fig. 2; it consisted of the contact between a glass lens (BK7 Plano Convex Lens SLB-30-400P, SIGMAKOKI) and a PDMS block (SYLGARD®184 SILICONE ELASTOMER KIT, Dow Corning). The glass lens ($R_1 = 207.6$ mm) was attached to a clear acrylic plate that was fixed to the motorized stage (KZL06075-C1-GA, SURUGA SEIKI). The PDMS block (60 × 60 × 10 mm) was placed on the digital balance (strain gauge type TE612-L, Sartorius). The gross displacement Z was manipulated by the motorized stage, and the force F and contact radius a were measured simultaneously by using the digital balance and microscope (SKM-3000B-PC, SAITOH KOUGAKU). The spring constant k of the equivalent stiffness of the measurement system was measured to $k = 10.5$ kN/m as shown in Fig. 3.

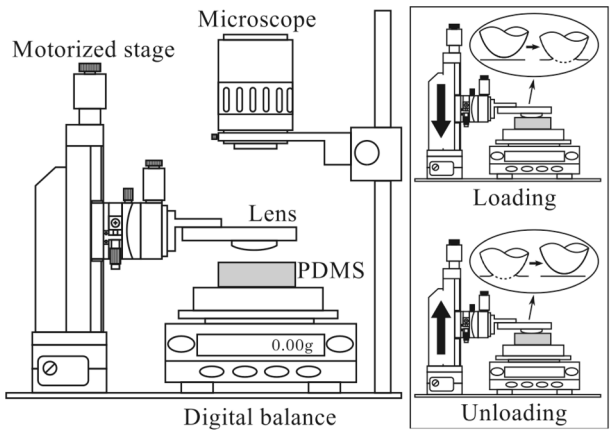

Fig. 2 Schematic illustration of the measurement system (*left*) and loading–unloading processes (*right*). The gross displacement was controlled by the motorized stage, and the force and contact area were measured by using the digital balance and microscope

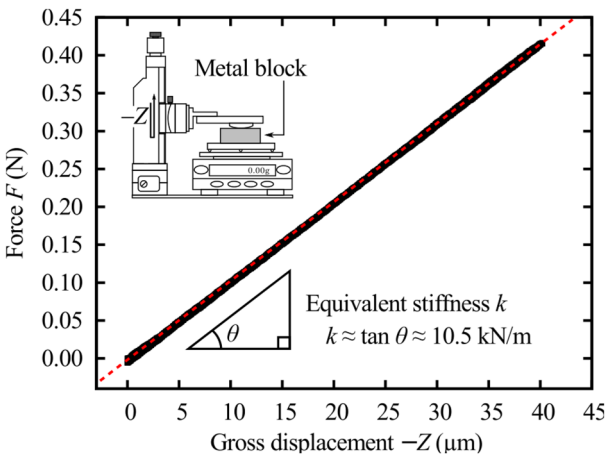

Fig. 3 Measurement of the equivalent stiffness *k* of the measurement system. The PDMS block in Fig. 2 was replaced to the metal block for the measurement of *k*. The loading–unloading of the gross displacement *Z* was tested in the speed of motorized stage at 0.1 μm/s, and both of the loading–unloading are plotted. The result shows that a hysteresis in the measurement system is small enough to be negligible. Therefore, the equivalent stiffness was determined to $k = 10.5$ kN/m from the gradient as shown

The PDMS mixture for the PDMS block was made with a mixing ratio of 10:1 of the base polymer and curing agent for fully cross-linked rubber. The air bubbles in the mixture were removed through degassing in a desiccator under a vacuum of 2 kPa for 1 h. The degassed mixture was poured carefully into a mold (60 × 60 × 20 mm) that had a clean glass bottom for making the PDMS block surface smooth and flat. After the mold was filled with the mixture to about 10 mm high, the air bubbles were removed again for 10 min in the desiccator. The filled mold was cured in an oven at 60 °C for 12 h, and then the PDMS block was removed from the mold. The exposed side of the PDMS block in the heat curing was carefully glued to a glass slide (100 × 100 mm) with the same PDMS mixture. The sample was cured again in the oven at 60 °C for 12 h, and the PDMS block was permanently set on the glass slide. The glass lens and PDMS block were cleaned

using an ultrasonic cleaner with ethanol and dried using a nitrogen spray gun. After 24 h from the setting of samples to the measurement system in a clean bench on a vibration isolation table, the experiment was conducted at the ambient conditions of 20 °C with 50% humidity.

Experimental procedure

The gross displacement Z was manipulated in step-by-step movements with a constant dwell time in every step for evaluating the spontaneous energy dissipation at a fixed Z. The amount of movement between steps was set at 1 μm (the speed of the motorized stage was set at 1 μm/s). The dwell time for every step was set at 15 s. The loading process was performed up to the maximum loading displacement ($-Z_{max}$). After the loading process completed, the unloading process was performed until the lens detached. A dependence of the maximum loading displacement on the adhesion hysteresis has been reported [16, 20]. Hence, three different maximum loading displacement were chosen: $-Z_{max} = 10, 20, 30$ μm, which is sufficiently smaller than the thickness of the PDMS block 10 mm.

Results and discussions

Experimental results and adhesion hysteresis

The experimental results of $-Z_{max} = 10, 20, 30$ μm are plotted in Fig. 4. Adhesion hysteresis was observed between the loading–unloading paths in each result, and the larger hysteresis loop was observed in the larger $-Z_{max}$. Moreover, the calculation results of the force $F(Z, a)$ in Eq. (5) are plotted, which are calculated by substituting the measurements of Z and a into $F(Z, a)$. In the calculation, the effective radius of curvature was given as $R = R_1 = 0.2076$ m (i.e., the surface of the PDMS block was assumed flat) and the equivalent stiffness was given as $k = 10.5$ kN/m. The elastic modulus was determined to $E^* = 2.67$ MPa using the method of least squares between the calculated $F(Z,$

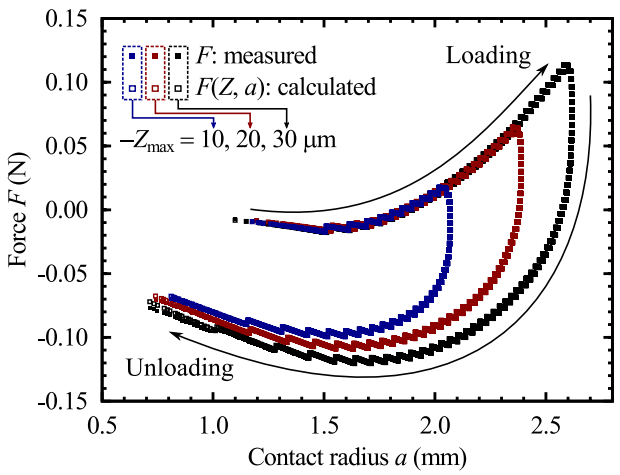

Fig. 4 The loading–unloading curve of $-Z_{max} = 10, 20, 30$ μm. The measured force F and calculated force $F(Z, a)$ are plotted as a function of the measured contact radius a. The calculated forces is calculated by substituting the measurements of Z and a into $F(Z, a)$ of Eq. (6); $R = 0.2076$ m, $k = 10.5$ kN/m, and $E^* = 2.67$ MPa with an RMSE between $F(Z, a)$ and F was 0.6 mN

a) and the measured F using entire measurements of $-Z_{max} = 10, 20, 30$ μm; the root mean square error (RMSE) between $F(Z, a)$ and F was 0.6 mN, which is small enough throughout the entire observed range of the force (−120 to 120 mN). Notably, the spring deformation calculated by Eq. (4) was 10 μm ($\approx -Z - \delta$) when the maximum force was applied ($F \approx 0.1$ N at $-Z_{max} = 30$ μm in Fig. 3).

At each fixed Z (15 s dwell time) the changing of F and a is observed in Fig. 4, and the changing in entire process is fitted well with the calculated force $F(Z, a)$ by Eq. (5) with the constant elastic modulus E^*. This result suggests that the PDMS block behaves as an elastic material in the contact process. Also, adhesion hysteresis between the loading–unloading paths represents that the total energy is not in equilibrium state. Therefore, it can be considered that the energy dissipation is induced in the contact interface, not in the PDMS block, from a spontaneous process of the total energy toward an equilibrium at each fixed Z, i.e., the spontaneous energy dissipation.

Strain energy release rate and work of adhesion

The work of adhesion $\Delta\gamma$ should be estimated for evaluating the total energy dissipation using Eq. (11). As shown in Eq. (10), G_Z consists of the work of adhesion and a dissipative term. Since the equilibrium of the total energy is given as $G_Z = \Delta\gamma$ and the total energy is spontaneously stabilized at fixed Z: G_Z tends to increase to become $\Delta\gamma$ in the loading process; G_Z tends to decrease to become $\Delta\gamma$ in the unloading process (until the existence of equilibrium) [10]. Figure 5 shows the calculation result of G_Z by Eq. (6). In the loading process, an approximately constant value of G_Z is observed at the end of each step with the advancing of contact radius a; on the contrary in the unloading process G_Z drastically changes with the receding of a. From the observation, we assume that the approximately constant value of G_Z observed at the end of each step in the loading process is close to the equilibrium $G_Z = \Delta\gamma$. Therefore, the approximately constant value is estimated to the work of adhesion $\Delta\gamma = 0.03$ J/m^2, which is a quite similar value

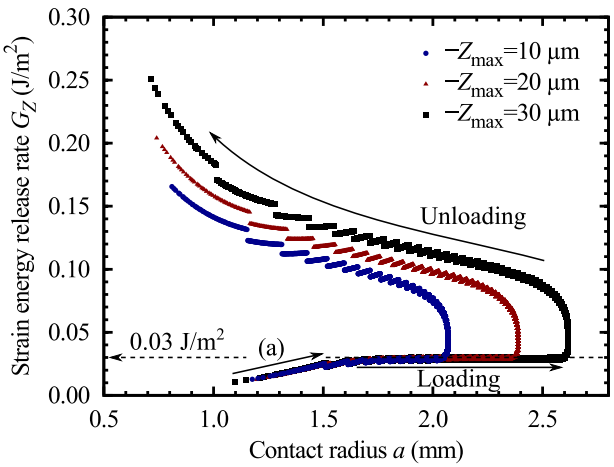

Fig. 5 Strain energy release rate G_Z as a function of the contact radius a. An approximately constant value of G_Z at the end of each step is observed in the loading process; on the contrary, in the unloading process, G_Z varies with the receding of a. The approximated value of 0.03 J/m^2 at the end of each step in the loading process is estimated to the work of adhesion $\Delta\gamma$. The initial contact of the first step is shown as a

obtained in [20]. Notice that the rapidly changing area marked with (a) in Fig. 5 represents the total energy is quite unstable when the initial contact is formed, thus, (a) is not suitable to the estimation.

Evaluation of energy dissipation

The energy dissipation is induced in the contact interface from a spontaneous process of the total energy toward an equilibrium at each fixed Z (15 s dwell time). And this relationship is also shown in Eq. (1) that $\Delta U_{\text{total}} = -\Delta U_{\text{dissipation}}$. Therefore, it can be considered that the total energy dissipation $U_{\text{dissipation}}$ calculated by Eq. (11) is a cumulative result of ΔU_{total} at each fixed Z during 15 s in entire contact process.

Figure 6 shows $U_{\text{dissipation}}$ as a function of contact radius a. In the loading process, the total energy dissipation $U_{\text{dissipation}}$ is little increased. In the unloading process, it is found that $U_{\text{dissipation}}$ is observed to be linearly proportional to the contact radius a. The gradient of $U_{\text{dissipation}}$ in a is expressed from using Eq. (1) and Eq. (10) as

$$-\frac{\partial U_{\text{dissipation}}}{\partial a} = \frac{\partial U_{\text{total}}}{\partial a} = 2\pi a(G_Z - \Delta\gamma), \tag{12}$$

which represents the gradient of U_{total} in a determined at each fixed Z. For convenience, we call the gradient using a character f in this paper. Figure 7 shows the gradient f of $-U_{\text{dissipation}}$ (or U_{total}) as a function of a calculated by Eq. (12). An approximately constant f is observed for each unloading process, i.e., $f = 0.71$ mJ/m ($-Z_{\max} = 10$ μm), $f = 0.83$ mJ/m ($-Z_{\max} = 20$ μm), $f = 1.03$ mJ/m ($-Z_{\max} = 30$ μm). This result represents that the gradient f is determined as a roughly constant value during the receding contact, and f has a dependency on the maximum loading displacement $-Z_{\max}$.

The total energy dissipation and the gradient show that the contact process is not in equilibrium. Although the occurrence mechanism of the spontaneous energy dissipation is not clear, Fig. 5 shows that the total energy could not be fully stabilized state

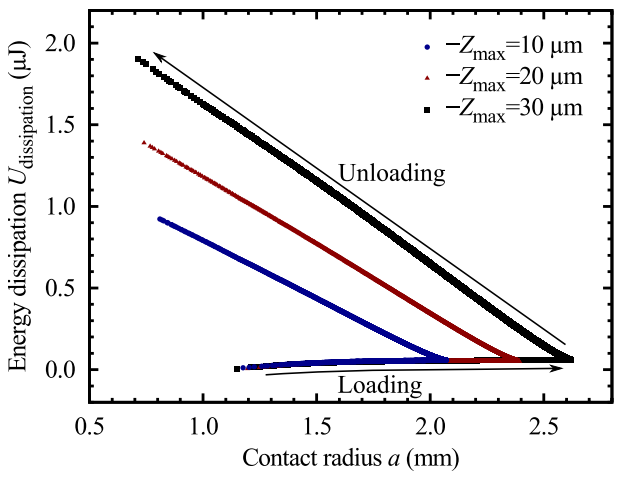

Fig. 6 Total energy dissipation $U_{\text{dissipation}}$ as a function of contact radius a. Linearity between $U_{\text{dissipation}}$ and a is observed in the unloading process (receding contact)

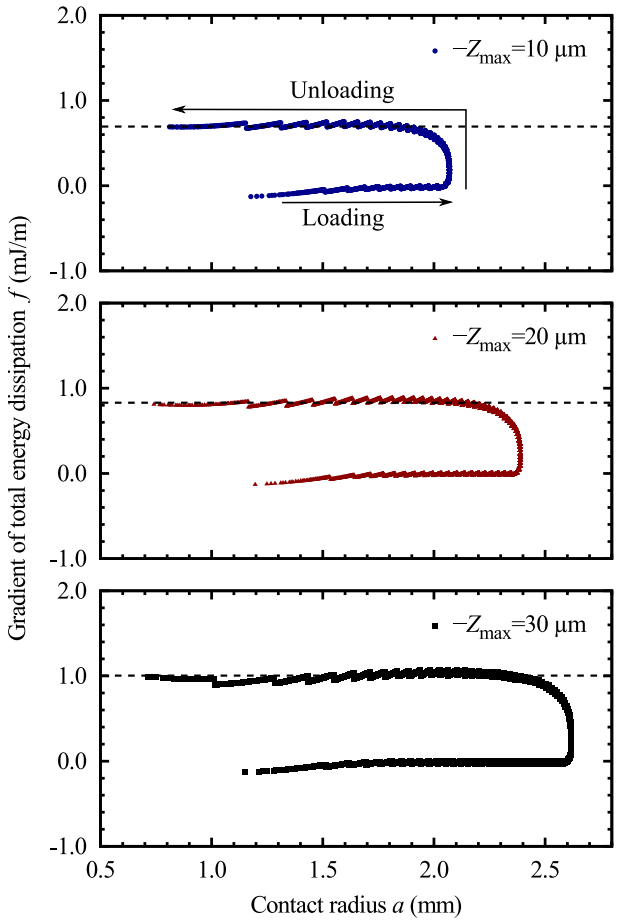

Fig. 7 Gradient of total energy dissipation f as a function of contact radius a. An approximately constant value of the gradient f is obtained in the unloading process (receding contact): $f = 0.71$ mJ/m ($-Z_{max} = 10$ μm), $f = 0.83$ mJ/m ($-Z_{max} = 20$ μm), $f = 1.03$ mJ/m ($-Z_{max} = 30$ μm)

($G_Z = \Delta\gamma$) at a fixed Z within 15 s especially in the unloading, i.e., the amount of spontaneous energy dissipation $\Delta U_{\text{dissipation}}$ at a fixed Z is limited within the dwell time. A not fully stabilized total energy affect a next step as a history by the step-by-step control of Z in every 15 s. In the larger maximum loading displacement $-Z_{max}$, the more step is required to detach the lens from the PDMS, and it can be considered that the more history might be accumulated. Therefore, the larger value of gradient f is observed in the larger $-Z_{max}$ because of the accumulated history related to the amount of required step in the unloading process.

As expressed in Eq. (12), the gradient of total energy dissipation is calculated using $G_Z - \Delta\gamma$ (the dissipative term that the reversible term $\Delta\gamma$ is excluded from the required energy to change unit contact area G_Z) and $2\pi a$ (the entire length of the crack tip). The dimension of the gradient f is J/m, and is also expressed as the dimension of the force N. In this paper, therefore, we define f as a dissipative force which is applied to $2\pi a$ during the receding contact. From this, it can be considered that the dissipative force would be induced by an unknown factor existed at the crack tip $2\pi a$. An unknown factor might be an adsorbate on the surface gathered by $-Z_{max}$, such as gases, liquids, uncross-linked

PDMS fragments or etc. Although the mechanism is not clear, the approximately constant f and the dependency on $-Z_{\max}$ observed in Fig. 7 suggests a hint how an unknown factor works at the crack tip $2\pi a$.

Conclusion

The energy dissipation is evaluated in the contact process between the glass lens and the PDMS block. The experiments with the three maximum loading displacement $-Z_{\max}$ were conducted. The results (Fig. 4) shows that the adhesion hysteresis would be occurred even using the elastic material (PDMS block). This suggests that the mechanism would be induced by some interfacial phenomena. Furthermore, it is found that the approximately constant gradient f (Fig. 7) of the total energy dissipation (Fig. 6) which has a dependency on $-Z_{\max}$. This fact would suggest that the dissipative force f (the gradient) is possibly induced by an unknown factor existed at the crack tip $2\pi a$ gathered by $-Z_{\max}$, e.g., an adsorbate on the material surface.

Abbreviations

PDMS: polydimethylsiloxane; G, G_Z: strain energy release rate; $\Delta\gamma$: work of adhesion; U: energy; F: applied force; δ: penetration depth; a: contact radius; Z: gross displacement; R: effective radius of curvature; R_1, R_2: radius of curvature; E: young's modulus; ν: poisson's ratio; E^*: elastic modulus; k: equivalent stiffness; $-Z_{\max}$: maximum loading displacement; f: gradient of total energy dissipation (or dissipative force).

Authors' contributions

DB and KT designed the research. DB performed the experiments and analysis. All authors contributed to the results and discussions. PH, SS and KT supported for DB to write the manuscript. All authors read and approved the final manuscript.

Author details

[1] Department of International Development Engineering, Tokyo Institute of Technology, 2-12-1 O-okayama, Meguro-ku, Tokyo 152-8552, Japan. [2] Department of Transdisciplinary Science and Engineering, Tokyo Institute of Technology, 2-12-1 O-okayama, Meguro-ku, Tokyo 152-8552, Japan.

Acknowledgements

Not applicable.

Competing interests

The authors declare that they have no competing interests.

Received: 12 October 2016 Accepted: 24 January 2017
Published online: 03 February 2017

References

1. Geim AK, Dubonos SV, Grigorieva IV, Novoselov KS, Zhukov AA, Shapoval SY. Microfabricated adhesive mimicking gecko foot-hair. Nat Mat. 2003;2:461–3.
2. Murphy MP, Aksak B, Sitti M. Adhesion and anisotropic friction enhancements of angled heterogeneous micro-fiber arrays with spherical and spatula tips. J Adhes Sci Technol. 2007;21:1281–96.
3. Davies J, Haq S, Hawke T, Sargent JP. A practical approach to the development of a synthetic gecko tape. Int J Adhes Adhes. 2009;29:380–90.
4. Menon C, Murphy M, Sitti M. Gecko inspired surface climbing robots. In: ROBIO 2004. IEEE international conference on robotics biomimetics. 2004;431–6.
5. Kim S, Spenko M, Trujillo S, Heyneman B, Santos D, Cutkosky MR. Smooth vertical surface climbing with directional adhesion. IEEE Trans Robot. 2008;24:65–74.
6. Johnson KL, Kendall K, Roberts AD. Surface energy and the contact of elastic solids. Proc R Soc Lond Ser A. 1971;324:301–13.
7. Takahashi K, Mizuno R, Onzawa T. Influence of the stiffness of the measurement system on the elastic adhesional contact. J Adhes Sci Technol. 1995;9:1451–64.
8. Sekiguchi Y, Hemthavy P, Saito S, Takahashi K. Adhesion between side surface of an elastic beam and flat surface of a rigid body. J Adhes Sci Technol. 2012;26:2615–26.
9. Silberzan P, Perutz S, Kramer EJ, Chaudhury MK. Study of the self-adhesion hysteresis of a siloxane elastomer using the JKR method. Langmuir. 1994;10:2466–70.
10. Maugis D, Barquins M. Fracture mechanics and the adherence of viscoelastic bodies. J Phys D Appl Phys. 1978;11:1989–2023.

11. Ahn D, Shull KR. Effects of substrate modification on the interfacial adhesion of acrylic elastomers. Langmuir. 1998;14:3646–54.
12. Shull KR. Contact mechanics and the adhesion of soft solids. Mat Sci Eng R. 2002;36:1–45.
13. Waters JF, Guduru PR. Mode-mixity-dependent adhesive contact of a sphere on a plane surface. Proc R Soc Lond Ser A. 2010;466:1303–25.
14. Deruelle M, Hervet H, Jandeau G, Leger L. Some remarks on JKR experiments. J Adhes Sci Technol. 1998;12:225–47.
15. She H, Malotky D, Chaudhury MK. Estimation of adhesion hysteresis at polymer/oxide interfaces using rolling contact mechanics. Langmuir. 1998;14:3090–100.
16. Lorenz B, Krick BA, Mulakaluri N, Smolyakova M, Dieluweit S, Sawyer WG, Persson BN. Adhesion: role of bulk viscoelasticity and surface roughness. J Phys Condens Matter. 2013;25:225004.
17. Chen YL, Helm CA, Israelachvili JN. Molecular mechanisms associated with adhesion and contact angle hysteresis of monolayer surfaces. J Phys Chem. 1991;95:10736–47.
18. Israelachvili J. Interfacial forces. J Vac Sci Technol A. 1992;10:2961–71.
19. Pickering JP, Van Der Meer DW, Vancso GJ. Effects of contact time, humidity, and surface roughness on the adhesion hysteresis of polydimethylsiloxane. J Adhes Sci Technol. 2001;15:1429–41.
20. Kesari H, Lew AJ. Effective macroscopic adhesive contact behavior induced by small surface roughness. J Mech Phys Solids. 2011;59:2488–510.
21. Sekiguchi Y, Hemthavy P, Saito S, Takahashi K. Experiments of the adhesion behavior between an elastic beam and a substrate. Int J Adhes Adhes. 2014;49:1–6.
22. Grobelny J, Pradeep N, Kim DI, Ying ZC. Quantification of the meniscus effect in adhesion force measurements. Appl Phys Lett. 2006;88:091906.
23. Erath J, Schmidt S, Fery A. Characterization of adhesion phenomena and contact of surfaces by soft colloidal probe AFM. Soft Matter. 2010;6(7):1432–7.
24. Butt HJ, Barnes WJP, Del Campo A, Kappl M, Schönfeld F. Capillary forces between soft, elastic spheres. Soft Matter. 2010;6(23):5930–6.
25. Contreras-Naranjo JC, Ugaz VM. A nanometre-scale resolution interference-based probe of interfacial phenomena between microscopic objects and surfaces. Nat Commun. 2013;4:1–9.
26. Muller VM, Yushchenko VS, Derjaguin BV. On the influence of molecular forces on the deformation of an elastic sphere and its sticking to a rigid plane. J Colloid Interface Sci. 1980;77:91–101.
27. Maugis D. Adhesion of sphere: the JKR-DMT transition using a dugdale model. J Colloid Interface Sci. 1992;150:243–69.
28. Dupré MA. Théorie mécanique de la chaleur. Paris: Gauthier-Villars; 1869.